Supplementary Materials: Surface Heat Budget over the North Sea in Climate Change Simulations — Supplementary Material

Christian Dieterich [1,*], Shiyu Wang [1], Semjon Schimanke [1], Matthias Gröger [1], Birgit Klein [2], Robinson Hordoir [1,3], Patrick Samuelsson [1], Ye Liu [1], Lars Axell [1], Anders Höglund [1] and H. E. Markus Meier [1,4]

1. Model Description

1.1. Open Boundary Conditions

For the current setup of NEMO-Nordic climatological monthly profiles of sea surface height (SSH) are prescribed along the open boundaries along ∼4 °W and along ∼59 °N. The SSH has been taken from a historical run with the global ocean model MPIOM [1] and is prescribed for RCA4-NEMO ERA40 hindcast runs. The SSH from the MPIOM run is a 50-year climatological mean for the years 1960 to 2009. To allow for higher volume transports across the open boundary of NEMO-Nordic the SSH profiles have been deformed to reflect the bathymetry and resolution used in NEMO-Nordic. Sensitivity studies with the Hamburg Shelf Ocean Model HAMSOM by Mathis *et al.* [2] have shown that the profile of SSH prescribed as boundary conditions are of major importance for the circulation in the North Sea .

The mean sea level in global ocean models rises due to different processes and the sea level in the regional ocean model co-varies as it is prescribed as a boundary condition. What is more relevant dynamically, is the gradients in sea level along the open boundaries of the regional ocean model. These gradients determine the transport across the boundary and thus the means of communication between the regional ocean model and the outside world. When the outside is represented by an ERA40 hindcast the SSH on the open boundary of NEMO-Nordic is prescribed as a climatological monthly profile adapted from a historical MPIOM run. For the scenario simulations the boundary conditions on the open boundary of NEMO-Nordic ought to reflect changes going on in the global ocean models. These changes include dynamical changes due to circulation changes in atmosphere and ocean plus the diagnosed thermosteric expansion. Not included are the addition of mass due to glacier and ice sheet melting or changes in land water storage [3]. Also the glacial isostatic adjustment has not been taken into account for the construction of the boundary conditions. The profiles of absolute SSH are then taken from the OGCM output and treated in the same way as the SSH for the hindcast runs to increase the normal transports. All the sea level gradients on the boundary exhibit strong seasonal, interannual and decadal variability during the 21st century. Even though the sea level itself increases on the boundary over the course of the century mean transports change only slightly compared to the variability. Only the sea level across the Norwegian Coastal Current and the sea level difference between the Fair Isle Current and the inflow through the English Channel tend to increase by ∼5 cm. The increased transport in the Norwegian Coastal Current is likely to be caused by an increased freshwater signal from the European continent (see below) and the changing balance between inflows through the Fair Isle Current and the English Channel might reflect changes in the circulation in the North East Atlantic.

In the present setup the volume transport across the open boundaries is calculated according to Flather [4] given the prescribed profiles of SSH. Additionally, eleven tidal harmonic constituents (M2, S2, N2, K2, K1, O1, P1, Q1, M4, MS4, MN4) from the tidal model for the European Shelf [5] are prescribed to allow the North Sea to resonate. For temperature and salinity climatological monthly sections from Janssen *et al.* [6] are used as boundary conditions along the open boundaries for the ERA40 hindcast runs. For the scenario simulations temperature and salinity are sampled from the

OGCMs and prescribed as monthly mean sections. Temperature and salinity are subject to a flow relaxation scheme [7] that also calculates the normal baroclinic velocities on the open boundary.

1.2. River Discharge

All RCA4-NEMO experiments use the same daily runoff based on a simulation with the hydrological model E-HYPE [8]. E-HYPE was driven with ERA-interim data downscaled by RCA4 for the period 1979 to 2008. During this period the daily runoff is used directly as boundary conditions to NEMO-Nordic. Prior to that (1961 to 1978) a daily climatology of the runoff is applied. For the scenario period 2006 (2001 for the SRES scenario) to 2099 the daily climatology is prescribed for most of the rivers. Only for the Bothnian Sea and Bothnian Bay we increase the runoff linearly by +10% at the end of the century. This is done in accordance with a projected increase in precipitation in the northern Baltic Sea [e.g. 9,10]. In total, 424 river mouth locations are implemented into the model system. Some 220 are located in the Baltic Sea, roughly 50 in the Kattegat and Belt Sea and the remaining 150 discharge into the North Sea. The averaged river discharge amounts to $\sim$16400 m^3/s into the Baltic Sea and 13000 m^3/s into the North Sea which is in the range of observations [11]. In this version of RCA4-NEMO the river water from all rivers enter the ocean model without carrying any momentum and with the same temperature as in the adjacent ocean. The salinity of river water is set to 1 mg/kg.

Due to positive net precipitation (precipitation minus evaporation) plus river discharge the Baltic Sea has on average a positive water balance which leads to a freshwater outflow. The mean outflow for the period 1970 to 1999 for the different RCA4-NEMO experiments varies between 17670 m^3/s (EC-EARTH) and 20550 m^3/s (ECHAM5 20C). The outflow of the ERA40 run amounts to 17890 m^3/s. The lower figures are higher than the observations, e.g. 16115 m^3/s by Meier and Kauker [12], while the upper limit severely overestimates the freshwater surplus. One reason is a overestimation of river discharge in the E-HYPE data. Reports on river discharge range from 14085 to 15053 m^3/s [12] and 13600 m^3/s [13] depending on, e.g. the period analyzed and the method used.

However, another contribution to the overestimation of the freshwater surplus is due to net precipitation. The RCA4-NEMO simulation with the largest freshwater surplus (ECHAM5 20C) has a net precipitation of $\sim$3700 m^3/s averaged over the Baltic Sea for the period 1970 to 1999. In the ERA40 run net precipitation is 1300 m^3/s during the same period, while other studies report a net precipitation of 1530 m^3/s [13] and 2030 m^3/s [14]. Too much net precipitation in RCA4-NEMO leads to the high amount of freshwater outflow from the Baltic Sea in the current model setup. The net precipitation in RCA4-NEMO is strongly dependent on the driving GCM. The large freshwater outflow from the Baltic Sea contributes to the low sea surface salinity in the Norwegian Coastal Current (cf. Section 2).

1.3. Parameterizations

For NEMO-Nordic we use penetrative solar radiation split up into three spectral bands according to Lengaigne *et al.* [15], Morel [16]. Only a part of the shortwave radiation is taken up at the surface. Another portion penetrates into the water column and is absorbed in different depths depending on the attenuation properties of the water. In the case of an ecosystem model coupled to the physical model the attenuation of light could be predicted using the concentration of phytoplankton and yellow matter [17,18]. In the current version of NEMO-Nordic we use one single water type for the entire model domain. According to Aarup [19] the Secchi depth in the North Sea and Baltic Sea varies between less than 1 m in the German Bight to 15 m and more in the Norwegian Trench and the western Baltic Sea. Neglecting spatial and temporal variations in Secchi depth we assume a constant Secchi depth of 9 m for the whole model domain. That translates into a depth of the euphotic zone of $\sim$18 m [19]. With the three band model of Lengaigne *et al.* [15] the target depth of the euphotic zone is approximated by three evenly partitioned contributions that reach down to 11 m for red, 23 m for green and 31 m for blue light.

To balance the momentum flux applied at the air-sea interface the model ocean is subject to no-slip conditions along the lateral walls and to quadratic friction on the ocean floor. The drag coefficient is calculated according to the law of the wall with a roughness length of 1 cm and varies between $5 \cdot 10^{-4}$ and $8 \cdot 10^{-3}$. A bottom boundary layer (BBL) according to Döscher and Beckmann [20] covers the bottom grid cells to parametrize density driven flow along the bathymetry. We use a diffusivity of 1000 m^2/s in the BBL and assume the advective contributions to vanish. This is probably less relevant for the North Sea but more so for the exchange of water through the Danish Straits and the subsequent flow over the sills into the deeper basins of the Baltic Sea. Subgrid scale mixing of momentum and tracers is implemented with an isopycnal background viscosity and diffusivity of 0.2 m^2/s, respectively using a harmonic operator. Extra lateral viscosity with coefficients calculated following Griffies and Hallberg [21], Smagorinsky [22] helps to reduce the variance on small spatial scales and limit high current velocities in the upper water column along the coast of Norway and in the Åland Sea. Along the open boundaries a sponge zone of about 0.75 °width is implemented where the viscosity increases quadratically from 0.2 m^2/s to 200 m^2/s towards the open boundary.

Vertical mixing in the water column is parametrized using the general length scale implementation of the $k - \epsilon$ turbulence model [23]. Following Burchard and Bolding [24], Bolding *et al.* [25] we use lower limits for the turbulent kinetic energy (k_{min} = 10^{-6} m^2/s^2) and the dissipation rate (ϵ_{min} = 10^{-12} m^2/s^3) to account for unresolved processes. As suggested by Burchard and Bolding [24] we use flux boundary conditions for turbulent kinetic energy and dissipation rate. To diagnose viscosity and diffusivity the stability functions of Canuto *et al.*'s (2001) model A are applied as proposed by Bolding *et al.* [25].

A time step that satisfies the different criteria for numerical stability in topographic gradient, friction, mixing, advection and wave propagation turns out to be of the order of 180 s with a barotropic sub-step of 10 s.

1.4. Initial Conditions

All the model runs with the RCM have been started from an atmosphere and an ocean at rest, initialized with representative profiles for the active tracers. The first nine years 1961 to 1969 are used to spin up the system. For the Baltic Sea with a freshwater residence time of 35 years [14] that is a short time span and the deep Baltic Sea might not be in a quasi stationary state after the spin up. For the North Sea where vertical mixing homogenizes the whole water column during winter a spin up of one year would be sufficient [27]. Since there is no multi-year ice in the Baltic Sea a spin up of one year is adequate for the ice model. The atmosphere only needs a couple of weeks to spin up, but to equilibrate e.g. soil moisture may take several years [e.g. 28,29].

2. Model Validation

2.1. Evaluation of SSS

The downscaled runs GFDL-ESM2M, HadGEM2-ES and IPSL-CM5A-MR are too fresh. The different mean SSSs among the experiments can be attributed partly to the different amount of volume transport in the Norwegian Coastal Current (Tab. S1) and the freshwater outflow from the Baltic Sea (Fig. S1). The most important factor is the vertical distribution of freshwater in the outflow from the Baltic Sea, however. The freshwater height in the Norwegian Coastal Current is similar in all the experiments (not shown) and amounts to ∼6 m off Kristiansand compared to ∼5 m put forward by Gustafsson and Stigebrandt [30]. One reason for the model bias in freshwater height is the somewhat drier conditions in the period 1950 to 1990 where the bulk of data was available for Gustafsson and Stigebrandt's (1996) study.

The cause for too low averaged SSS in the ocean only ERA40 hindcast is the very fresh surface water in the outflow of the Baltic Sea. The amount of freshwater is similar to the coupled ERA40 hindcast but the vertical distribution is different (not shown). In the coupled ERA40 hindcast the freshwater penetrates deeper into the water column. This is due to differing fluxes between atmosphere and ocean between these two model runs. Most likely the amount of energy in the wind (Fig. S4) that translates into turbulent kinetic energy in the mixed layer of the ocean leads to deeper mixing of surface freshwater. This argument applies also to differences in averaged SSS among the historical periods of the scenario experiments.

SSS tends to be within $\pm$ 0.5 g/kg of the climatological annual mean of the ICES climatology (Fig. S1) and the KNSC dataset (not shown) which are derived basically from the same observations. An exception are the outflow from the Baltic Sea and the discharge from the river mouths of the largest rivers in the North Sea. To some extent the resolution in the gridded data might not be sufficient to resolve the freshwater tongues that form downstream of these river mouths. That would lead to fresh bias in the model results. It is likely however, that the harmonic operator used to implement subgrid scale mixing of tracers and momentum is not capable to parametrize the complex dynamics in these regions. The combined river outlets of Rhine/Meuse/Scheldt/Ijssel and the Ems/Jade/Weser/Elbe tend to have a regional impact in the Southern Bight and in the German Bight, respectively. All model solutions are much too fresh along the Dutch coast. In the German Bight there is a more complex, but consistent pattern of SSS biases compared to the ICES climatology. The consistency among the model solutions indicates that model deficiencies are responsible for the SSS biases along the continental coast. Mixing by eddies and baroclinic instability are not properly resolved and these processes are mostly represented as parameterizations. In sensitivity runs it was observed that mixing along geopotential levels improves the sea surface salinity in the eastern part of the North Sea substantially over the standard ERA40 hindcast that uses isopycninc mixing. Further improvements were found with a biharmonic mixing scheme over a harmonic operator. More importantly the outflow of the Baltic Sea is too fresh by up to 3 g/kg along the coast of Norway. The large fresh biases are confined mostly to the region north of the 100 m isobath. In Section 1 we argued that the too large freshwater export from the Baltic Sea affects the SSS in the Norwegian Coastal Current. Additionally, weak transports (Tab. S1) towards the north across the open boundary seem to inhibit the removal of freshwater from the outflow region of the Baltic Sea.

2.2. Circulation and Volume Transport

By means of Fig. S2 some of the major features of the depth averaged circulation in the North Sea can be identified. There is a broad southward flow around 0 °E that recirculates in several loops first to the east and then back to the north which may be identified with the Dooley Current. The currents (and transports) in the Fair Isle Current at the northwestern model boundary are rather weak in this model setup. Further south the British coastal water flows eastward through the Silver Pit and is joined by Channel water. One branch of the circulation follows northeastward in a broad band and then turns northward to follow approximately the 40 m isobath. At around 57 °N most of the flow retroflects eastward to feed the Jutland Current. Another part of the current flows to northwest between the 100 m and 200 m isobaths where it meets the southeastward flowing Atlantic water. The Norwegian Coastal Current is visible as a narrow band of high velocities along the coast of Norway. Overall, the circulation reflects the well known cyclonic circulation in the North Sea.

Table S1 summarizes volume transports across representative sections in the North Sea. Across the sections in the English Channel there is between 0.12 and 0.21 Sv entering the North Sea in the different model solutions. Otto *et al.* [31] list a volume transport of 0.10 to 0.17 Sv. Compared to the value of 0.094 Sv measured by Prandle *et al.* [32] however, the inflow from the English Channel is nearly double the observed volume flow for most of the model solutions. The ERA40 hindcast using a climatological monthly SSH on the open boundary (cf. Section 1) is the model run with the least amount of overestimation. The GCMs used on the boundaries of the RCM tend to overestimate the transport through the English Channel, except for the GFDL and IPSL models.

As laid out in Section 1 the Baltic Sea outflow is overestimated in the RCA4-NEMO ERA40 hindcasts as well as in the historical periods of the scenario simulations (cf. section N9 in Tab. S1). The recirculation in the Skagerrak, Jutland Current plus the inflow in the Norwegian Trench to the east and the outflow in the Norwegian Coastal Current amount to 0.5 to 0.6 Sv with slightly higher outflow due to the addition of the Baltic Sea outflow in the Norwegian Coastal Current. Estimates by Danielssen *et al.* [33] for the inflow and outflow of Atlantic water in the Skagerrak are of the order of 1.0±0.5 Sv.

The inflow of water from the Atlantic across 59 °N is rather low in our model setup. Since the transport is de facto prescribed as a boundary condition there is room for improvement to adjust the normal transports across the open boundaries of the model domain. On the other hand it is the GCMs that provide the information on transports in and out of the North Sea. If the RCM cannot overcome the shortcomings of the GCM then the classical approach to a regional model with prescribed transports at its open boundaries reaches its limits. Solutions that allow the transport into the North Sea be determined in a consistent way [1,2,34,35] are more promising then.

Generally, the underestimation of meridional volume transports across the open boundaries of the regional ocean model will lead to an underestimation of the oceanic, advective contribution to the lateral heat transport in the heat budget of the North Sea.

2.3. Sensitivity of Volume Transports

A series of sensitivity experiments was conducted that focused on the influence of the open boundary condition in the ocean component, mainly the one in the northern North Sea. The aim was to understand whether the boundary conditions can be adjusted to improve the inflow from and the outflow to the Atlantic. In a first step the climatology for T, S and SSH was replaced by the ORAS4 reanalysis [36]. From this reanalysis monthly mean values for T, S and SSH were interpolated onto the open boundary of the ocean component. This lead to somewhat smaller biases in SSS and to somewhat larger transports across the open boundary and a stronger recirculation in the Skagerrak as indicated in Tab. S1 (cf. ERA40 and ORAS4). The procedure described in Section 1 was applied to the ORAS4 data to account for the higher resolution of the regional model. In the next step the barotropic transport was determined from the monthly ORAS4 reanalysis and used in the open boundary condition [4]. This was a major improvement both for transports across the open boundary and for the salinity bias (experiment ORAS4 b). The recirculation in the Skagerrak increases to 0.8 Sv which is within the estimate of Danielssen *et al.* [33] of 1.0±0.5 Sv. The transport in the NCC increases to around 1 Sv. That is in agreement with observations. In the region affected by the Baltic Sea outflow a bias reduction for SSS of more than 1 g/kg was observed for this experiment. A further increase in the mean transports is seen when hourly SSH and transports from a storm surge model are applied additionally on the open boundary conditions. This experiment is listed as ORAS4 c in Table S1. Two additional experiments Surge and Surge b use only the hourly output of the storm surge model without any mean SSH or transports from the ORAS4 reanalysis or Janssen *et al.*'s (1999) climatology. The transports are very weak in both cases and are clearly insufficient to drive a realistic North Sea circulation. The experiment Surge b uses the same data as the experiment Surge, but the years 1979 to 2009 have been shuffled randomly. This was intended to test whether the barotropic signal traveling in from the North East Atlantic is relevant or whether it is just the variability in the northern North Sea.

The boundary conditions used in experiment ORAS4 b (and ORAS4 c) have improved the transports across the sections shown in Table S1 over the default model setup. What they did not improve is the tendency of a weak and too wide transport in the western part of the northern North Sea. A remodelling of the bathymetry, like opening up the closed wall between Scotland and the northern boundary along ∼4 °W, a less smoothed bathymetry in the northwestern part of the model domain and a relocation of the open boundary further north will be considered for future model setups. A number of model studies [e.g. 37–40] have shown that regional models of the North Sea are capable of realistically represent volume transports even in the vicinity of open boundaries. Model development for the present setup will need to improve on volume transports in the North Sea.

2.4. Validation of Wind Speed and Direction

Wind speed and direction time series exist locally for measurement stations as for instance the Marine Environmental Monitoring Network in the North Sea and Baltic Sea (MARNET) operated by the German Federal Maritime and Hydrographic Agency (BSH) or the FINO platforms. We use MARNET and FINO stations to validate wind speed and directions over the open North Sea.

The lowest measurements on FINO platforms is in 33 m height, so only wind direction can be used directly to compare with 10m wind from the atmosphere model. Wind speed is validated at two MARNET stations where the wind is quantified in 14m. In general, the ERA40 driven simulation does not set apart from the simulations driven with GCMs at the boundary. At both stations FINO1 (6.6 °E, 54.0 °N) and FINO3 (7.2 °E, N 55.2 °N) the model solutions overestimate westerly to southerly wind directions by up to 3 m/s. The overestimation of westerly to southerly winds is balanced by an underrepresentation of NW and NE winds (Fig. S3).

Fig. S4 illustrates the PDF distributions of the daily mean wind speeds in the model compared to the MARNET stations Deutsche Bucht (7.5 °E, 54.2 °N) and Ems (6.3 °E, 54.2 °N). Whereas high wind speeds of more than 14 m/s are underestimated wind speeds around 10 m/s are mainly overestimated. Part of this discrepancy is related to the height of the measurements. The wind speed is measured in 14 m at MARNET stations whereas model data is interpolated to 10 m. However, the discrepancy is also present for the SMHI stations along the coast of the Baltic Sea (not shown) which are taken at 10 m. Based on instantaneous values we find an underestimation of high wind speeds (>17 m/s) along the Swedish coast of the Baltic Sea as for the North Sea stations. This underestimation of high wind speeds has been reported also by Ganske *et al.* [41] who investigated thoroughly wind speed of RCMs over the North Sea.

2.5. Validation of SST and SSS

In a second part of the model validation results from the RCA4-NEMO ERA40 hindcast are compared to actual observations. Following Gröger *et al.* [42] the variability of the models temperature and salinity fields is compared to the Marine Environmental Data Base (MUDAB). During the period 1999 to 2008 monthly mean temperature and salinity were sampled from the model solution and compared to O(5000) measurements from the observational data base. To group the measurements the North Sea was subdivided into 155 boxes. More data were available during winter and summer than during spring and fall. Most measurements were taken at the surface. The number of available data points decreased gradually with depth.

During this ten-year period the variability in T and S in the model solution compares well to the observed one with a rms error of 1.3 °C (0.5 g/kg) and a correlation of 0.93 (0.87) for temperature (salinity). The standard deviation of the model temperature closely matches the observed one with a value of 1.1 °C for both. The variability in salinity is somewhat lower in the model solution with a standard deviation of 0.92 g/kg compared to a value of 1.05 g/kg in the observations.

1. Sein, D.V.; Mikolajewicz, U.; Gröger, M.; Fast, I.; Cabos, W.; Pinto, J.G.; Hagemann, S.; Semmler, T.; Jacob, D. Regionally coupled atmosphere - ocean - sea ice - marine biogeochemistry model ROM. Part I: Description and validation. *J Adv Model Earth Sy* **2015**, *7*, 268–304. doi:10.1002/2014MS000357.
2. Mathis, M.; Mayer, B.; Pohlmann, T. An uncoupled dynamical downscaling for the North Sea: Method and evaluation. *Ocean Model* **2013**, *72*, 153 – 166. doi:http://dx.doi.org/10.1016/j.ocemod.2013.09.004.
3. Church, J.A.; Clark, P.U.; Cazenave, A.; Gregory, J.M.; Jevrejeva, S.; Levermann, A.; Merrifield, M.A.; Milne, G.A.; Nerem, R.S.; Nunn, P.D.; Payne, A.J.; Pfeffer, W.T.; Stammer, D.; Unnikrishnan, A.S. Sea Level Change. In *Climate Change 2013: The Physical Science Basis. Contribution of Working Group I to the Fifth Assessment Report of the Intergovernmental Panel on Climate Change*; Stocker, T.F.; Qin, D.; Plattner, G.K.; Tignor, M.; Allen,

S.K.; Boschung, J.; Nauels, A.; Xia, Y.; Bex, V.; Midgley, P.M., Eds.; Cambridge University Press: Cambridge, United Kingdom and New York, NY, USA, 2013; chapter 13, pp. 1137–1216.

4. Flather, R.A. A Storm-Surge Prediction Model for the Northern Bay of Bengal with Apllication to the Cyclone Disaster in April 1991. *J Phys Oceanogr* **1994**, *24*, 172–190. doi:{10.1175/1520-0485(1994)024<0172:ASSPMF>2.0.CO;2}.
5. Egbert, G.D.; Erofeeva, S.Y.; Ray, R.D. Assimilation of altimetry data for nonlinear shallow-water tides: Quarter-diurnal tides of the Northwest European Shelf. *Cont Shelf Res* **2010**, *30*, 668–679. doi:10.1016/j.csr.2009.10.011.
6. Janssen, F.; Schrum, C.; Backhaus, J.O. A Climatological Data Set of Temperature and Salinity for the Baltic Sea and the North Sea. *Hydrogr Z* **1999**, *Supplement*, 245 pp.
7. Engedahl, H. Use of the flow relaxation scheme in a three-dimensional baroclinic ocean model with realistic topography. *Tellus A* **1995**, *47*, 365–382. doi:10.1034/j.1600-0870.1995.t01-2-00006.x.
8. Donnelly, C.; Andersson, J.C.M.; Arheimer, B. Using flow signatures and catchment similarities to evaluate the E-HYPE multi-basin model across Europe. *Hydrolog Sci J* **2016**, *61*, 255–273. doi:10.1080/02626667.2015.1027710.
9. Meier, H.E.M.; Müller-Karulis, B.; Andersson, H.C.; Dieterich, C.; Eilola, K.; Gustafsson, B.G.; Höglund, A.; Hordoir, R.; Kuznetsov, I.; Neumann, T.; Ranjbar, Z.; Savchuk, O.P.; Schimanke, S. Impact of Climate Change on Ecological Quality Indicators and Biogeochemical Fluxes in the Baltic Sea: A Multi-Model Ensemble Study. *Ambio* **2012**, *41*, 558–573. doi:10.1007/s13280-012-0320-3.
10. Donnelly, C.; Yang, W.; Dahné, J. River discharge to the Baltic Sea in a future climate. *Climatic Change* **2014**, *122*, 157–170. doi:10.1007/s10584-013-0941-y.
11. Bergström, S.; Carlsson, B. River runoff to the Baltic Sea - 1950-1990. *Ambio* **1994**, *23*, 280–287.
12. Meier, H.E.M.; Kauker, F. Sensitivity of the Baltic Sea salinity to the freshwater supply. *Clim Res* **2003**, *24*, 231–242. doi:10.3354/cr024231.
13. Omstedt, A.; Axell, L.B. Modeling the variations of salinity and temperature in the large Gulfs of the Baltic Sea. *Cont Shelf Res* **2003**, *23*, 265–294.
14. Meier, H.E.M.; Kauker, F. Modeling decadal variability of the Baltic Sea: 2. Role of freshwater inflow and large-scale atmospheric circulation for salinity. *J Geophys Res* **2003**, *108*, 3368. doi:10.1029/2003JC001799.
15. Lengaigne, M.; Menkes, C.; Aumont, O.; Gorgues, T.; Bopp, L.; André, J.M.; Madec, G. Influence of the oceanic biology on the tropical Pacific climate in a coupled general circulation model. *Clim Dynam* **2007**, *28*, 503–516. doi:10.1007/s00382-006-0200-2.
16. Morel, A. Optical modeling of the upper ocean in relation to its biogenous matter content (case I waters). *J Geophys Res* **1988**, *93*, 10749–10768. doi:10.1029/JC093iC09p10749.
17. Kuznetsov, I.; Eilola, K.; Dieterich, C.; Hordoir, R.; Axell, L.; Höglund, A.; Schimanke, S. Model study on the variability of ecosystem parameters in the Skagerrak-Kattegat area, effect of load reduction in the North Sea and possible effect of BSAP on Skagerrak–Kattegat area. Oceanografi 119, SMHI, 2016.
18. Löptien, U.; Meier, H.E.M. Simulated distribution of colored dissolved organic matter in the Baltic Sea. Oceanografi 109, SMHI, 2011.
19. Aarup, T. Transparency of the North Sea and Baltic Sea - a Secchi depth data mining study. *Oceanologia* **2002**, *44*, 323–337.
20. Döscher, R.; Beckmann, A. Effects of a Bottom Boundary Layer Parameterization in a Coarse-Resolution Model of the North Atlantic Ocean. *J Atmos Ocean Tech* **2000**, *17*, 698–707. doi:10.1175/1520-0426(2000)017<0698:EOABBL>2.0.CO;2.
21. Griffies, S.M.; Hallberg, R.W. Biharmonic Friction with a Smagorinsky-Like Viscosity for Use in Large-Scale Eddy-Permitting Ocean Models. *Mon Weather Rev* **2000**, *128*, 2935–2946. doi:10.1175/1520-0493(2000)128<2935:BFWASL>2.0.CO;2.
22. Smagorinsky, J. General Circulation Experiments with the Primitve Equations: 1 the Basic Experiment. *Mon Weather Rev* **1963**, *91*, 99–164. doi:10.1175/1520-0493(1963)091<0099:GCEWTP>2.3.CO;2.
23. Madec, G. *NEMO ocean engine*. IPSL, Paris, France, 3.3 ed., 2011.
24. Burchard, H.; Bolding, K. Comparative Analysis of Four Second-Moment Turbulence Closure Models for the Oceanic Mixed Layer. *J Phys Oceanogr* **2001**, *31*, 1943–1968. doi:10.1175/1520-0485(2001)031<1943:CAOFSM>2.0.CO;2.

25. Bolding, K.; Burchard, H.; Pohlmann, T.; Stips, A. Turbulent mixing in the Northern North Sea: a numerical model study. *Cont Shelf Res* **2002**, *22*, 2707–2724. doi:http://dx.doi.org/10.1016/S0278-4343(02)00122-X.
26. Canuto, V.M.; Howard, A.; Cheng, Y.; Dubovikov, M.S. Ocean Turbulence. Part I: One-Point Closure Model–Momentum and Heat Vertical Diffusivities. *J Phys Oceanogr* **2001**, *31*, 1413–1426. doi:10.1175/1520-0485(2001)031<1413:OTPIOP>2.0.CO;2.
27. Pohlmann, T. Predicting the thermocline in a circulation model of the North Sea - Part 1: model description, calibration and verification. *Cont Shelf Res* **1996**, *16*, 131–146. doi:10.1016/0278-4343(95)90885-S.
28. Cosgrove, B.A.; Lohmann, D.; Mitchell, K.E.; Houser, P.R.; Wood, E.F.; Schaake, J.C.; Robock, A.; Sheffield, J.; Duan, Q.; Luo, L.; Higgins, R.W.; Pinker, R.T.; Tarpley, J.D. Land surface model spin-up behavior in the North American Land Data Assimilation System (NLDAS). *J Geophys Res-Atmos* **2003**, *108*. doi:10.1029/2002JD003316.
29. Yang, Y.; Uddstrom, M.; Duncan, M. Effects of short spin-up periods on soil moisture simulation and the causes over New Zealand. *J Geophys Res-Atmos* **2011**, *116*. doi:10.1029/2011JD016121.
30. Gustafsson, B.; Stigebrandt, A. Dynamics of the freshwater-influenced surface layers in the Skagerrak. *J Sea Res* **1996**, *35*, 39–53. doi:10.1016/S1385-1101(96)90733-9.
31. Otto, L.; Zimmerman, J.T.F.; Furnes, G.K.; Mork, M.; Saetre, R.; Becker, G. Review of the physical oceanography of the North Sea. *Neth J Sea Res* **1990**, *26*, 161–238. doi:10.1016/0077-7579(90)90091-T.
32. Prandle, D.; Ballard, G.; Flatt, D.; Harrison, A.J.; Jones, S.E.; Knight, P.J.; Loch, S.; McManus, J.; Player, R.; Tappin, A. Combining modelling and monitoring to determine fluxes of water, dissolved and particulate metals through the Dover Strait. *Cont Shelf Res* **1996**, *16*, 237–257. doi:10.1016/0278-4343(95)00009-P.
33. Danielssen, D.S.; Edler, L.; Fonselius, S.; Hernroth, L.; Ostrowski, M.; Svendsen, E.; Talpsepp, L. Oceanographic variability in the Skagerrak and Northern Kattegat, May-June, 1990. *ICES J Mar Sci* **1997**, *54*, 753–773. doi:doi: 10.1006/jmsc.1996.0210.
34. Marsland, S.J.; Haak, H.; Jungclaus, J.H.; Latif, M.; Röske, F. The Max-Planck-Institute global ocean/sea ice model with orthogonal curvilinear coordinates. *Ocean Model* **2003**, *5*, 91–127. doi:10.1016/S1463-5003(02)00015-X.
35. Holt, J.; Wakelin, S.; Lowe, J.; Tinker, J. The potential impacts of climate change on the hydrography of the northwest European continental shelf. *Prog Oceanogr* **2010**, *86*, 361–379. doi:10.1016/j.pocean.2010.05.003.
36. Balmaseda, M.A.; Mogensen, K.; Weaver, A.T. Evaluation of the ECMWF ocean reanalysis system ORAS4. *Q J Roy Meteor Soc* **2013**, *139*, 1132–1161. doi:10.1002/qj.2063.
37. Holt, J.; Proctor, R. The seasonal circulation and volume transport on the northwest European continental shelf: A fine-resolution model study. *J Geophys Res* **2008**, *113*. doi:10.1029/2006JC004034.
38. Su, J.; Sein, D.V.; Mathis, M.; Mayer, B.; O'Driscoll, K.; Chen, X.; Mikolajewicz, U.; Pohlmann, T. Assessment of a zoomed global model for the North Sea by comparison with a conventional nested regional model. *Tellus A* **2014**, *66*, 23927. doi:10.3402/tellusa.v66.23927.
39. Mathis, M.; Elizalde, A.; Mikolajewicz, U.; Pohlmann, T. Variability patterns of the general circulation and sea water temperature in the North Sea. *Prog Oceanogr* **2015**, *135*, 91–112. doi:10.1016/j.pocean.2015.04.009.
40. Pätsch, J.; Burchard, H.; Dieterich, C.; Gräwe, U.; Gröger, M.; Mathis, M.; Kapitza, H.; Bersch, M.; Moll, A.; Pohlmann, T.; Su, J.; Ho-Hagemann, H.T.M.; Schulz, A.; Elizalde, A.; Eden, C. An evaluation of the North Sea circulation in global and regional models relevant for ecosystem simulations. *Ocean Model* **2017**, *111*, 70–95. doi:https://doi.org/10.1016/j.ocemod.2017.06.005.
41. Ganske, A.; Tinz, B.; Rosenhagen, G.; Heinrich, H. Interannual and Multidecadal Changes of Wind Speed and Directions over the North Sea from Climate Model Results. *Meteorol Z* **2016**, *25*, 463–478. doi:10.1127/metz/2016/0673.
42. Gröger, M.; Maier-Reimer, E.; Mikolajewicz, U.; Moll, A.; Sein, D. NW European shelf under climate warming: implications for open ocean - shelf exchange, primary production, and carbon absorption. *Biogeosciences* **2013**, *10*, 3767–3792. doi:10.5194/bg-10-3767-2013.
43. Klein, H.; Lange, W.; Mittelstaedt, E. Tidal and Residual Currents in the Northern North Sea: Observations. *Dtsch Hydrogr Z* **1994**, *46*, 5–27. doi:10.1007/BF02225739.

List of Figures

S1 Climatological annual mean SSS biases (g/kg) for different RCA4-NEMO experiments relative to KNSC. ERA40 (upper row, left), Ensemble mean (upper row, middle), MPI-ESM-LR (upper row, right), EC-EARTH (middle row, left), GFDL-ESM2M (middle row, middle), HadGEM2-ES (middle row, right), IPSL-CM5A-MR (lower row, left), ECHAM5 (lower row, middle) and ocean only run (lower row, right). The averaging period for the model data and the observational data span the years 1970 to 1999. 10

S2 Climatological annual mean near surface currents (m/s) for the RCA4-NEMO ERA40 hindcast. The reference vector represents a velocity of 0.25 m/s. Only at every fourth grid point a vector is drawn. The colored section drawn in the figure are those where transports are sampled and listed in Tab. S1. The four stations for the wind roses and wind histograms in Figures S3 and S4 are marked as red triangles in the figure. 11

S3 Wind roses at stations FINO1 (left) and FINO3 (right) during the period September 2004 to September 2006. The black sectors in the figure represents the measurements at 33 m height and the colored sectors represent the statistics of the 10m wind from the model solutions: ERA40 hindcast (green), ECHAM5 (yellow), MPI-ESM-LR (blue) and EC-EARTH (red), respectively. 12

S4 Distribution of daily mean wind speed at stations Deutsche Bucht (left) and Ems (right) from MARNET during the period 1989 to 2006. The statistics of the observations at 14 m height yields the shaded area. The statistics derived from the downscaled 10m wind are displayed for the ERA40 hindcast (black), MPI-ESM-LR (red), EC-EARTH (green), GFDL-ESM2M (blue), HadGEM2-ES (yellow), IPSL-CM5A-MR (rose) and ECHAM5 (olive), respectively. 13

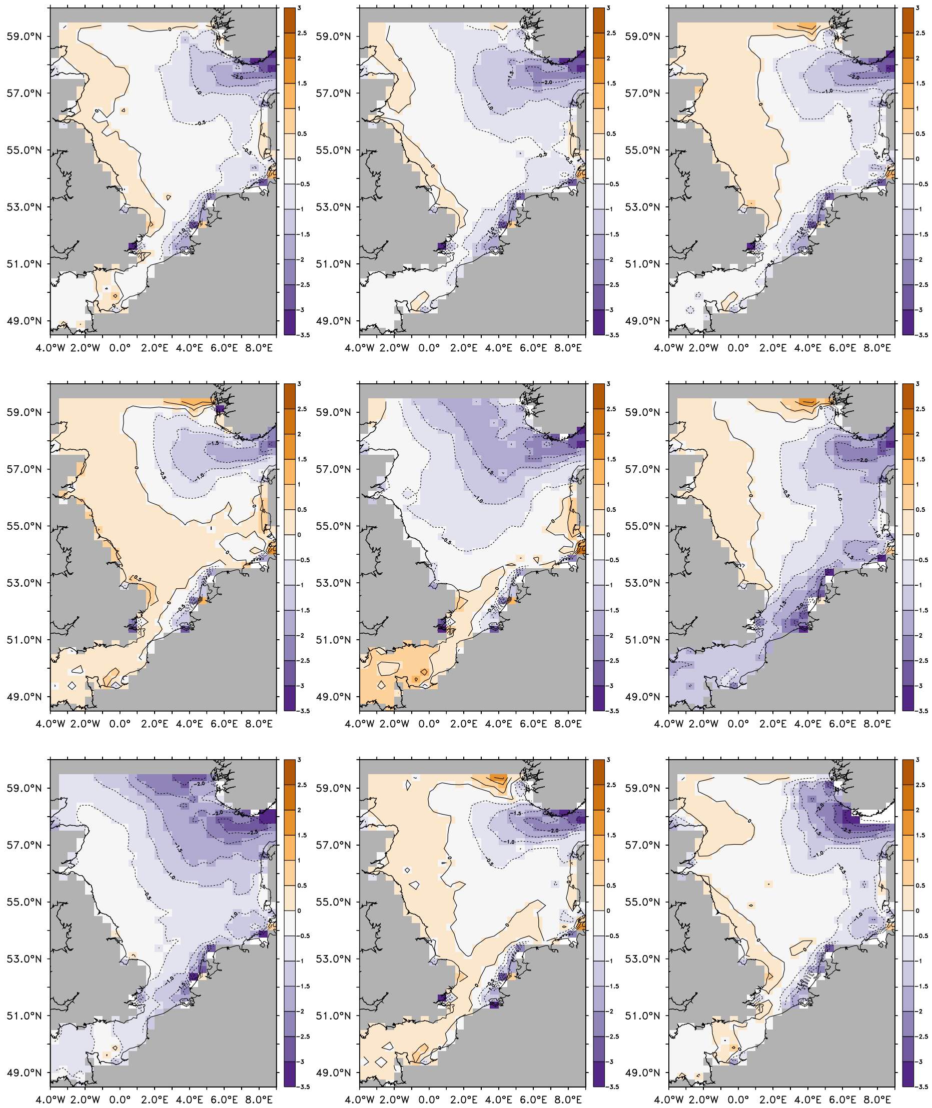

Figure S1. Climatological annual mean SSS biases (g/kg) for different RCA4-NEMO experiments relative to KNSC. ERA40 (upper row, left), Ensemble mean (upper row, middle), MPI-ESM-LR (upper row, right), EC-EARTH (middle row, left), GFDL-ESM2M (middle row, middle), HadGEM2-ES (middle row, right), IPSL-CM5A-MR (lower row, left), ECHAM5 (lower row, middle) and ocean only run (lower row, right). The averaging period for the model data and the observational data span the years 1970 to 1999.

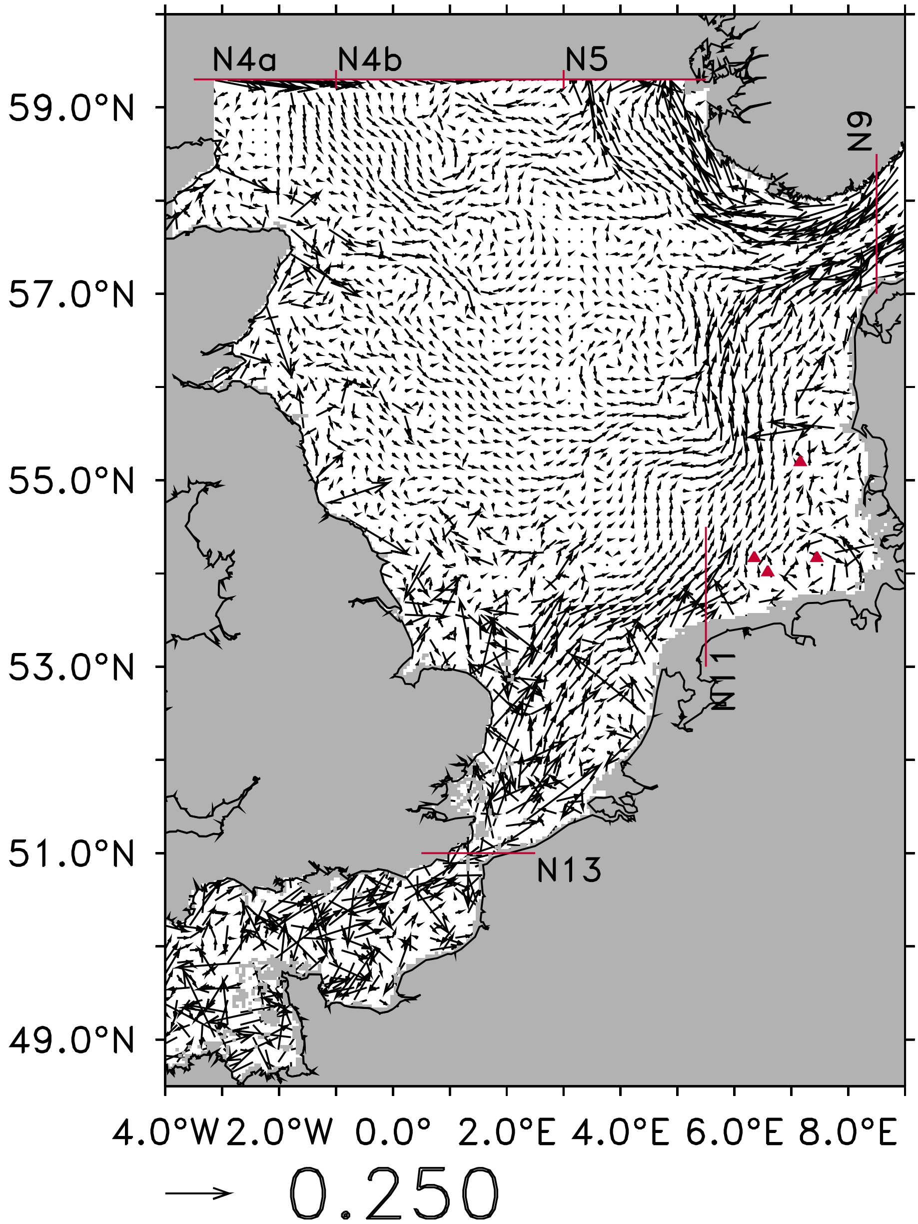

Figure S2. Climatological annual mean near surface currents (m/s) for the RCA4-NEMO ERA40 hindcast. The reference vector represents a velocity of 0.25 m/s. Only at every fourth grid point a vector is drawn. The colored section drawn in the figure are those where transports are sampled and listed in Tab. S1. The four stations for the wind roses and wind histograms in Figures S3 and S4 are marked as red triangles in the figure.

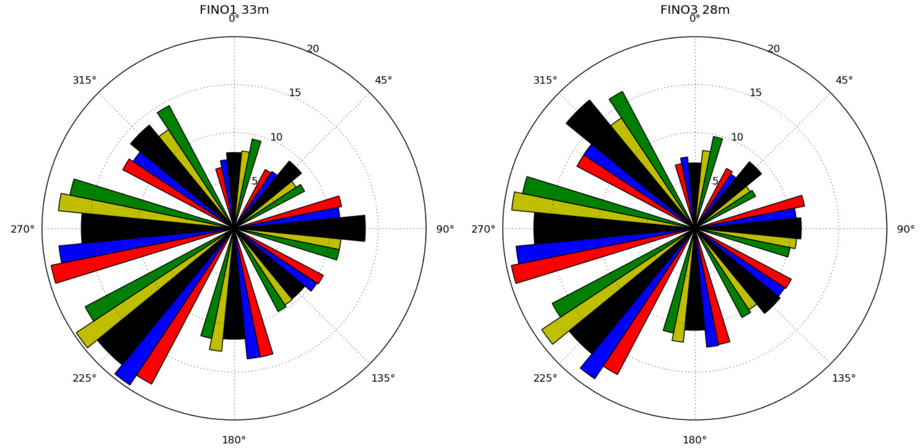

Figure S3. Wind roses at stations FINO1 (left) and FINO3 (right) during the period September 2004 to September 2006. The black sectors in the figure represents the measurements at 33 m height and the colored sectors represent the statistics of the 10m wind from the model solutions: ERA40 hindcast (green), ECHAM5 (yellow), MPI-ESM-LR (blue) and EC-EARTH (red), respectively.

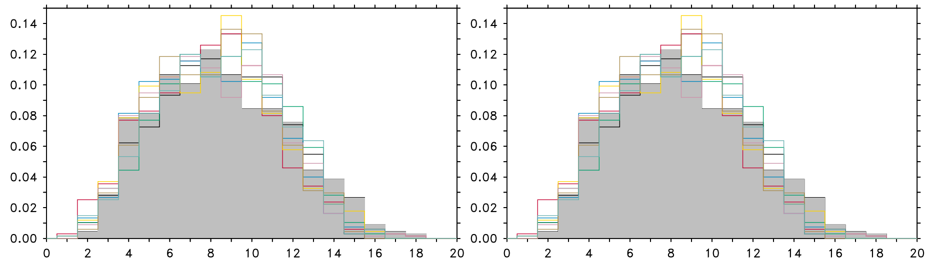

Figure S4. Distribution of daily mean wind speed at stations Deutsche Bucht (left) and Ems (right) from MARNET during the period 1989 to 2006. The statistics of the observations at 14 m height yields the shaded area. The statistics derived from the downscaled 10m wind are displayed for the ERA40 hindcast (black), MPI-ESM-LR (red), EC-EARTH (green), GFDL-ESM2M (blue), HadGEM2-ES (yellow), IPSL-CM5A-MR (rose) and ECHAM5 (olive), respectively.

List of Tables

S1 Summary of volume transports (Sv) during period P0 (1970-1999) for representative sections in the North Sea for hindcast and scenario experiments conducted with RCA4-NEMO. The names of the sections are based on the NOOS section network. N13 (Strait of Dover, 51 °N), N11 (Terschelling, 5.5 °E, 53 °N to 54.5 °N), N9 (Skagerrak, 8.5 °E), N4a (Fair Isle Current, 59.3 °N, 4 °W to 1 °W), N4b (Atlantic inflow, 59.3 °N, 1 °W to 3 °E), N5 (Norwegian Coastal Current, 59.3 °N, 3 °E to 6 °E), N4+5 (Orkney - Utsira, 59.3 °N, 4 °W to 6 °E). The eastward volume transport across section N9 is indicated in parentheses. For the NORA experiment (July to August, 1990) Klein *et al.* [43] calculated volume transports across 59 °N which are reproduced in the row NORA. Values given in row Obs. are the arithmetic mean values The lower part of the table shows the climatological volume transports (Sv) during the years 1980 to 2009. The row RCA4-NEMO shows results for the ERA40 hindcast. The remainder of the table list results from sensitivity experiments using the ocean only version of the model, driven with data from the coupled ERA40 hindcast. 15

Table S1. Summary of volume transports (Sv) during period P0 (1970-1999) for representative sections in the North Sea for hindcast and scenario experiments conducted with RCA4-NEMO. The names of the sections are based on the NOOS section network. N13 (Strait of Dover, 51 °N), N11 (Terschelling, 5.5 °E, 53 °N to 54.5 °N), N9 (Skagerrak, 8.5 °E), N4a (Fair Isle Current, 59.3 °N, 4 °W to 1 °W), N4b (Atlantic inflow, 59.3 °N, 1 °W to 3 °E), N5 (Norwegian Coastal Current, 59.3 °N, 3 °E to 6 °E), N4+5 (Orkney - Utsira, 59.3 °N, 4 °W to 6 °E). The eastward volume transport across section N9 is indicated in parentheses. For the NORA experiment (July to August, 1990) Klein *et al.* [43] calculated volume transports across 59 °N which are reproduced in the row NORA. Values given in row Obs. are the arithmetic mean values The lower part of the table shows the climatological volume transports (Sv) during the years 1980 to 2009. The row RCA4-NEMO shows results for the ERA40 hindcast. The remainder of the table list results from sensitivity experiments using the ocean only version of the model, driven with data from the coupled ERA40 hindcast.

	N13	**N11**	**N9**	**N4a**	**N4b**	**N5**	**N4+N5**
ERA40	0.16	0.13	-0.020 (0.57)	-0.19	-0.17	0.54	0.18
Ensemble mean	0.17	0.16	-0.020 (0.55)	-0.16	-0.09	0.44	0.19
MPI-ESM-LR	0.19	0.17	-0.021 (0.52)	-0.12	-0.09	0.44	0.23
EC-EARTH	0.20	0.17	-0.020 (0.56)	-0.17	-0.01	0.40	0.22
GFDL-ESM2M	0.14	0.14	-0.021 (0.53)	-0.21	-0.04	0.44	0.19
HadGEM2-ES	0.18	0.15	-0.019 (0.60)	-0.10	-0.21	0.52	0.21
IPSL-CM5A-MR	0.12	0.16	-0.022 (0.59)	-0.18	-0.08	0.42	0.16
ECHAM5	0.21	0.19	-0.024 (0.54)	-0.15	-0.04	0.45	0.26
NORA				-0.27	-0.14	0.72	0.32
Obs.	0.14		-0.017 (0.75)	-0.37	-0.41	0.67	0.11
RCA4-NEMO	0.17	0.14	-0.020 (0.59)	-0.18	-0.16	0.54	0.20
ERA40	0.18	0.12	-0.020 (0.57)	-0.16	-0.15	0.52	0.21
ORAS4	0.16	0.12	-0.021 (0.65)	-0.26	-0.17	0.62	0.19
ORAS4 b	0.16	0.12	-0.020 (0.82)	-0.16	-0.63	0.98	0.19
ORAS4 c	0.13	0.10	-0.021 (0.86)	-0.22	-0.71	1.09	0.16
Surge	0.07	0.08	-0.019 (0.46)	-0.10	-0.10	0.29	0.09
Surge b	0.07	0.08	-0.022 (0.46)	-0.10	-0.10	0.30	0.10